CHAPTER 7

INTEGRITY ASSESSMENT

The fracture parameters that are required for fatigue and fracture assessment were calculated in chapter 6. Chapter 5 is also strongly referenced for the section that deals with material properties(section 5.3). Three load categories were considered namely:

- Reverse bending stress due to gravity as the shaft rotates. This gives rise to a cyclic mode I stress intensity range, ΔK_I, that will result in fatigue if the material limit or fatigue threshold, $\Delta K_{I,th}$, is exceeded. The fatigue threshold is influenced by a number of factors including mixed mode loading and the stress ratio, R. The maximum in the range of ΔK_I also contributes towards final fracture when the material toughness, K_{IC}, is exceeded.
- Torque, due to power generation along the turbine train, gives rise to a steady mode III stress intensity, K_{III}. K_{III} has an influence on the fatigue threshold of the material and contributes to fracture.
- Shrink-on and frictional stress give rise to a steady mode I stress intensity, K_I. This stress category is associated with a gradient through the thickness of the shaft and has a much stronger influence on shallow cracks. K_I has an influence on the stress ratio and associated fatigue threshold.

All the required fracture parameters mentioned above were calculated in chapter 6 and must be interpreted to describe the predicted crack growth behaviour. The parameters were calculated for different friction assumptions and at different speeds. The solution at 0 rpm is used for the barring speed condition, which is at 70 rpm. Although the centrifugal influence at 70 rpm is negligible, the solution at 0 rpm gives a conservative lower bound and allows for further interpretation of reduced barring speeds without further calculations.

7.1. FATIGUE ASSESSMENT

If the cyclic stress intensity range exceeds the fatigue threshold during normal operation at 1500 rpm, a crack will grow very rapidly and reach a critical size in a fraction of the turbine operating cycle (between maintenance outages). This can be demonstrated by considering lower bound assumptions (slowest possible crack growth rate) with regard to the constants in the crack growth law, equation 5.4.4.

Neglecting the influence of multiaxial loading, the assumption of the lowest crack growth rate, case P1[L] in table 5.2 and a stress ratio of –1, throughout the range of crack growth, is made. The stress intensity range, ΔK_I, listed in table 6.5 is empirically described by the relation:

$$\Delta K_I = 0.7933 a^{0.527} \qquad (7.1.1)$$

where a is the crack size. Substituting the above assumptions into equation 5.4.4 gives a crack growth law as follows:

$$\frac{da}{dN}[\text{mm / cycle}] = \frac{1.69 \text{x} 10^{-8}}{\sqrt{2}} \left(0.7933 a^{0.527}\right)^{2.6} \qquad (7.1.2)$$

Numerical integration of equation 7.1.2 gives the crack growth curve illustrated in figure 7.1. The figure shows that an initial crack of 5 mm will grow to limits of the calculated data (200 mm crack) in 80 days at which stage the crack extension rate is in the order of 20 mm/day. It is evident that a crack that will propagate during normal operation renders the rotor inoperable and if no measures are in place to detect the crack at this stage, it will propagate until fracture occurs. Hence the importance of on-line detection.

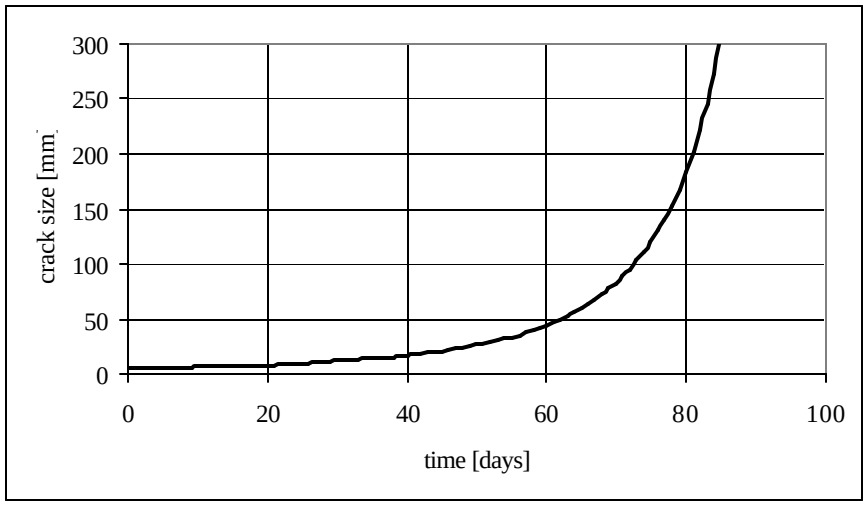

Figure 7.1: Graph of crack growth vs. time

It can be seen from the above argument that the shaft effectively reaches the end of its life when the fatigue threshold, at normal operating conditions, is exceeded. The crack size at which this will happen can be predicted by calculating the effective fatigue threshold given the different modes of loading that were calculated and listed in table 6.5.

The effective fatigue threshold can be calculated in accordance with equations 5.4.6 and 5.4.10. Table 7.2 shows the result of such a calculation for the case of friction release as well as for a friction coefficient of 0.3. Two cases of fatigue threshold values are covered (see discussion in section 5.4.3.1). They are 7 and 8 MPa.$m^{0.5}$, for an R value of zero, of which the latter is more likely to be representative of the actual material. Values were calculated at 0 and 1500 rpm covering all combinations of the data in table 6.5.

Figure 7.2 shows a graphical presentation of the results in table 7.1 for higher fatigue threshold value of 8 MPa.$m^{0.5}$. Figure 7.2 has a graph for each of the LP rotors because of the difference in torque. Figure 7.2 shows a curve for the effective applied stress intensity range (Applied K1 Range in legend). The figure also shows two other curves for the effective fatigue thresholds at 0 and 1500 rpm. Fatigue propagation will take place if the applied stress intensity range exceeds the effective threshold for a given condition. Table 7.3 shows a summary of the results in figure 7.2.

The results show that the crack, once initiated, will always propagate during barring operation. The graphs also show that a crack size of 72 mm and larger, depending on the rotor, will mark the onset of high cycle fatigue during normal operation.

A crack growth calculation, with the same constant as used in equation 7.1.2 but with the correct adjustment for R, was performed to investigate crack growth during barring operation. The rotors have been in barring operation for approximately 10 000 hr and the maximum crack depth is 15.6 mm. An initial crack size of 5 mm was used, assuming that initiation by fretting takes place during the first period of operation.

The curve predicts a crack depth of 12 mm after 10 000 hr of operation opposed to the actual value of 15.6. It is beyond the scope of this work to accurately predict the crack growth that occurs as a result of the initiation mechanism and the influence of the stress gradients in the key corners.

Figure 7.3 also shows the potential advantage of dropping the barring speed to 20 rpm for future operation. The crack growth rate drops significantly and the prediction is that the shaft can operate for a further extended period of operation, likely to the end of the power station's life, without any cracks propagating by high cycle fatigue.

a	K_I	K_I	ΔK_I	R	R	K_{III}	K_{III}	K_{III}	ΔK_{th} [0 rpm]	ΔK_{th} [1500 rpm]			ΔK_{th} [0 rpm]	ΔK_{th} [1500 rpm]		
	0	1500		0	1500				[7 MPa.m$^{1/2}$ at R=0]				[8 MPa.m$^{1/2}$ at R=0]			
[mm]	rpm	rpm		rpm	rpm	LP 1	LP 2	LP 3	0 rpm	LP 1	LP 2	LP 3	0 rpm	LP 1	LP 2	LP 3
5	12.00	4.70	3.59	0.74	0.45	0.00	0.00	0.00	2.52	4.46	4.46	4.46	2.88	5.10	5.10	5.10
25	6.70	3.00	6.50	0.35	-0.04	6.69	7.60	8.50	5.07	7.63	7.76	7.91	5.79	8.60	8.71	8.84
50	3.50	0.43	11.34	-0.24	-0.86	8.50	12.40	16.30	8.23	11.80	12.65	13.93	9.40	13.30	14.01	15.10
100	1.10	0.42	16.68	-0.77	-0.90	11.26	17.43	23.60	10.79	12.27	13.93	16.48	12.33	13.75	15.12	17.32

Table 7.2.a: Fatigue threshold values with friction release

a	K_I	K_I	ΔK_I	R	R	K_{III}	K_{III}	K_{III}	ΔK_{th} [0 rpm]	ΔK_{th} [1500 rpm]			ΔK_{th} [0 rpm]	ΔK_{th} [1500 rpm]		
	0	1500		0	1500				[7 MPa.m$^{1/2}$ at R=0]				[8 MPa.m$^{1/2}$ at R=0]			
[mm]	rpm	Rpm		rpm	rpm	LP 1	LP 2	LP 3	0 rpm	LP 1	LP 2	LP 3	0 rpm	LP 1	LP 2	LP 3
5	16.03	8.84	3.59	0.80	0.66	0.00	0.00	0.00	2.07	3.07	3.07	3.07	2.37	3.51	3.51	3.51
25	9.50	6.20	6.50	0.49	0.31	6.69	7.60	8.50	4.20	5.66	5.77	5.90	4.80	6.36	6.46	6.58
50	8.60	4.40	11.34	0.21	-0.13	8.50	12.40	16.30	5.88	8.27	9.06	10.14	6.72	9.28	9.95	10.90
100	2.60	2.00	16.68	-0.52	-0.61	11.26	17.43	23.60	9.65	10.92	12.52	14.92	11.02	12.21	13.55	15.64

Table 7.2.b: Fatigue threshold values without friction release

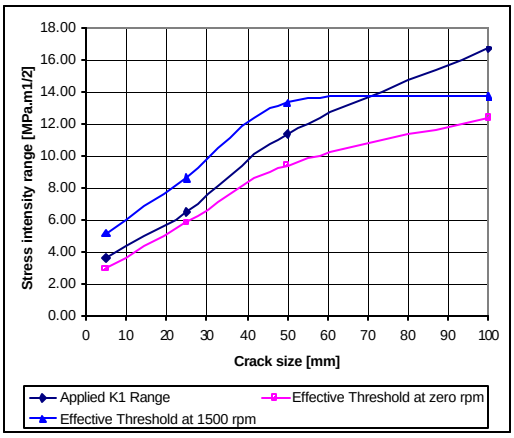

Figure 7.2.a: LP 1 Curves

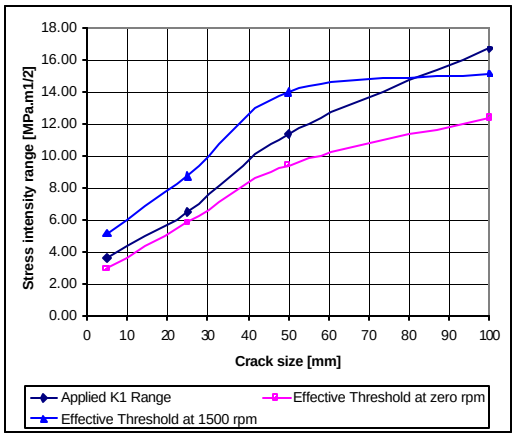

Figure 7.2.b: LP 2 Curves

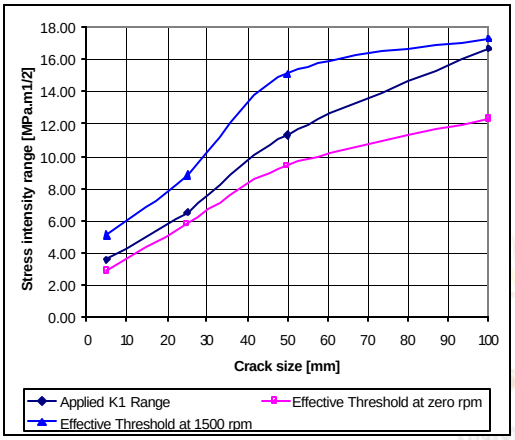

Figure 7.2.c: LP 3 Curves

Component	Fatigue threshold crack size at 1500 rpm
LP 1	72 mm
LP 2	82 mm
LP 3	> 100 mm

Table 7.3: Summary of results

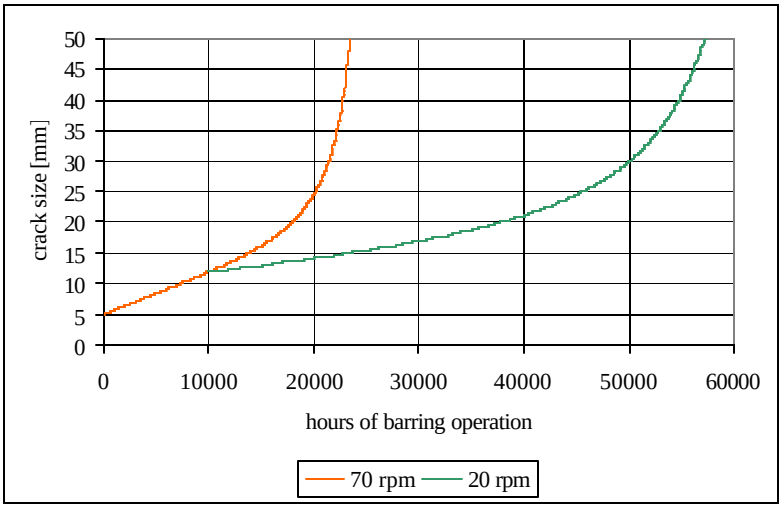

Figure 7.3: Crack growth during barring operation

7.2. FRACTURE ASSESSMENT

The purpose of fracture assessment, for this case, is to verify that the turbine can tolerate relatively large cracks. This is a requirement to ensure on-line detection of propagating crack and safe shutdown of the plant before the crack reaches a critical size.

It is virtually impossible to predict the dynamic loads once the rotor experiences increased vibration levels as a result of the presence of a crack. This aspect must be managed by an appropriate safety factor. Industry experience has, however, shown that cracks in excess of half the shaft diameter did not fracture so that the units could be shut down in time.

The maximum applied mode I stress intensity at the crack front is made up of the peak bending load and the shrink load as follows:

$$K_{I,max} = K_I + \Delta K_I/2 \qquad (7.2.1)$$

Table 6.5 indicates that K_I strives to zero for increasing crack depth. This was only confirmed for crack depths up to 100 mm because of the calculation effort involved. The solutions do show clear signs of stress redistribution. Following the logic that the compression in the rotor core is a result of the tension on the surface (see axi-symmetric result) and that the surface tension is released by deflection of the crack face, the core compression will also release. The core compression is a reaction to the surface tension. It is assumed that the trend will continue so that the steady state mode I stress intensity is zero for crack depths in excess of 100 mm.

With K_I in equation 7.2.1, the equivalent stress intensity is calculated in accordance with equation 5.4.5 as:

$$K_{eq} = \sqrt{\left(\frac{\Delta K_I}{2}\right)^2 + \frac{K_{III}^2}{(1-\nu)}} \qquad (7.2.2)$$

Using the values for a 470 mm crack as calculated in chapter 6 for LP3 gives:

$$K_{eq} = \sqrt{(29.7)^2 + \frac{38.9^2}{0.7}} = 55.2 \ \text{MPa.m}^{0.5}$$

This is well below the material toughness of 110 MPa.m$^{0.5}$. In reality the shaft operates at approximately 200 °C where the material toughness is in the region of 200 MPa.m$^{0.5}$ (see chapter 5). Figure 7.4 shows the calculated effective stress intensities for the parameters calculated in chapter 6.

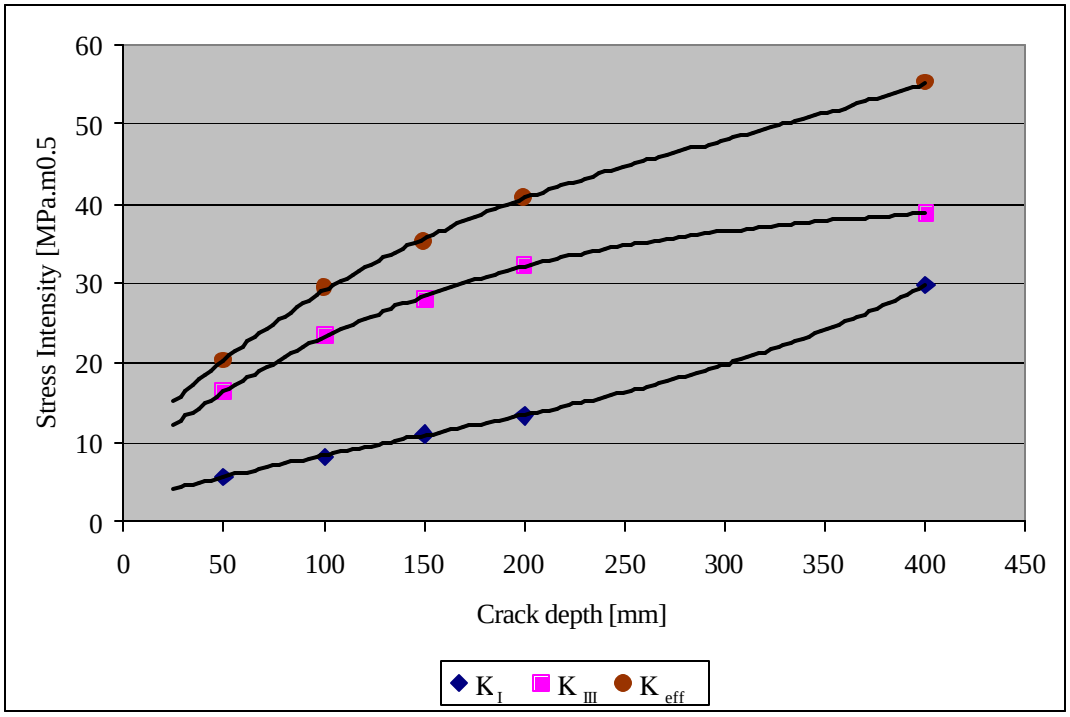

Figure 7.4: Effective stress intensity as a function of crack depth for LP3.

7.3. CONCLUSIONS

The fatigue and fracture assessment demonstrates the following:

- A crack, once initiated, will always propagate during barring operation for all crack sizes.
- The effective fatigue threshold is influenced by the applied torque during normal operation so that short cracks will arrest. Each LP rotor has a theoretical crack size that will mark the onset of HCF depending on the torque that it transmits. These crack sizes are 72, 82 and >100 mm for LPs 1, 2 and 3 respectively.
- The critical crack size for fracture is very large. This is demonstrated by the fact that the effective applied stress intensity for a 400 mm crack in this 940 mm shaft is still well below the material limit.